

Mathematical Modeling of the Autodyne Signal Characteristics at Strong Reflected Emission

Vladislav Ya. Noskov, Kirill A. Ignatkov, and Andrey P. Chupakhin

Ural Federal University named after the First President of Russia B.N.Yeltsin,
The Department of radioelectronics and information technology,
Yekaterinburg, Russia
noskov@oko-ek.ru,

Abstract. On the base of developed mathematical model of microwave oscillator interaction with the strong reflected emission, with attraction of numerical methods, the research results are presented for the features of the autodyne signal characteristics formation. Researches are fulfilled for the microwave oscillator model with a single-circuit oscillating system, taking into account its non-isochronity and non-isodromity. An influence of inherent parameters and the reflected emission delay phenomenon onto the autodune response formation is revealed. Graphs of normalized signal characteristics are obtained showing the autodyne response shape, and its spectral analysis is performed. Harmonic coefficients and amplitudes of spectrum harmonic components are calculated together with averaged value levels of the autodyne response as a function of reflection coefficient modulus at various distance of the radar object.

Keywords: autodyne, microwave oscillator, strong reflected emission, autodyne response, mathematical modeling of signals.

1 Introduction

Research results of autodyne microwave oscillator (MO) at strong reflected emission represent the practical interest in various areas of science and engineering. They are claimed at determination of output signal formation features, at estimation of the dynamic range, for analysis of parameter measurement errors and for a choice of the optimal operation mode of the short-range radar sensors, which use the autodyne principle of the transceiver architecture.

Specifics of these sensor functioning at problem solution, for instance, determination of electric-physical and dynamic parameters of the radar objects consists in the fact that the distance between a sensor and an object can be extremely small (down to zero) under several conditions. At that, the reflected emission level may turn out to be commensurable with the level of probing emission. In contrast to the enough studied case of the weak reflected emission, the case of the MO impact of strong emission was investigated insufficiently. It is examined in the known literature on the base of experimental data and modeling results on the analog computers only [1, 2].

In this paper, on the base of developed mathematical model with involving of numerical approaches, we present the analysis results of the single-circuit autodyne, which partially fill a mentioned gap.

2 Mathematical model of the autodyne at strong reflected emission

The functional block diagram of the radar sensor with the autodyne architecture principle of the transceiver is presented in fig. 1. Electromagnetic oscillations produced by MO are emitted through the receiving-transmitting antenna towards the radar object. Microwave emission reflected from the object returns through the same antenna into MO and causes the autodyne effect.

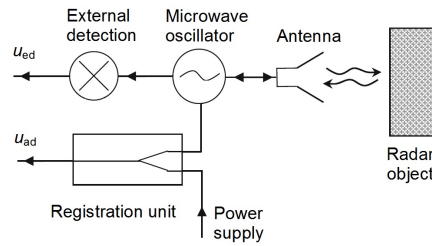


Fig. 1. Functional block diagram of the autodyne MO

As we know [1], the autodyne effect consists in variations of amplitude and a frequency of MO oscillations. At that, arisen autodyne variations of the current in the power source circuit of the MO active element (AE) are transformed into the auto-detection signal u_{ad} by means of the registration unit. In some autodyne sensor constructions, the useful signal is obtained with the help of external detection circuit u_{ed} , which transforms the autodyne variations of an amplitude or frequency of microwave oscillations to the output signal voltage.

The equivalent diagram of the autodyne MO can be represented in the form of parallel connection of averaged (over the oscillation period) AE conductivity $Y_{AE} = Y_{AE}(A, \omega)$, depended on the amplitude A and the current frequency ω of oscillations, the oscillating system (OS) $Y_{OS}(\omega)$ and the load $Y_L = Y_L(\omega)$. Oscillation equation for this circuit has a form [1, 3]:

$$Y_{AE}(A, \omega) + Y_{OS}(\omega) + Y_L(\omega) . \quad (1)$$

A difficulty of analytical solution finding of this equation consist in the presence of nonlinear dependences of all its terms upon oscillation parameters. At that, we should note that the $Y_L(\omega)$ conductivity in (1) also depends on the delay time τ of the emission, at that

$$Y_L(\omega) \equiv Y_L(\omega, \tau) = G_L(\omega, \tau) + jB_L(\omega, \tau) . \quad (2)$$

Here

$$G_L(\omega, \tau) = \frac{G_0(1 - \Gamma^2)}{1 + \Gamma^2 + 2\Gamma \cos \delta(\omega, \tau)} ,$$

$$B_L(\omega, \tau) = \frac{2G_0\Gamma \sin \delta(\omega, \tau)}{1 + \Gamma^2 + 2\Gamma \cos \delta(\omega, \tau)} ;$$

Γ is a modulus of the reflection coefficient reduced to MO terminals, which characterizes the emission attenuation at its propagation to the radar object and back; $\delta(\omega, \tau)$ is the total phase incursion; G_0 is the load conductivity at reflected emission absence.

To simplify analysis of (1) without loss of generality, we take some assumptions. We shall limit the present research by the case of autodyne response extraction of oscillation amplitude variation with the help of the external detector.

In addition, we shall examine the processes in MO in the form of variations of oscillation parameters in the vicinity of its steady-state, when at $\Gamma = 0$ we have: $A = A_0$, $\omega = \omega_0$. For this, we represent the oscillation amplitude and frequency in the form: $A = A_0 + \Delta A$, $\omega = \omega_0 + \Delta\omega$ where ΔA and $\Delta\omega$ are appropriate variations of the MO steady-state at $\Gamma \neq 0$.

Then, acting in accordance the accepted approach [1], from (1) with account of (2) for the case of MO with single-circuit OS, we obtain the system of linearized equations for determination of relative amplitude variations $a = \frac{\Delta A}{A_0}$ and the frequency of oscillation $\chi = \frac{\Delta\omega}{\omega_0}$:

$$\alpha a + \varepsilon \chi + \Gamma \eta \frac{\Gamma - \cos \delta(\omega, \tau)}{1 + \Gamma^2 + 2\Gamma \cos \delta(\omega, \tau)} = 0 ; \quad (3)$$

$$\beta a + Q_L \chi + \Gamma \eta \frac{\sin \delta(\omega, \tau)}{1 + \Gamma^2 + 2\Gamma \cos \delta(\omega, \tau)} = 0 , \quad (4)$$

where $\alpha, \varepsilon, \beta$ are dimensionless parameters determining the limit cycle strength, non-isodromity and non-isochronity of MO, relatively [4]; $\eta = \frac{G_0}{G}$ is an efficiency and Γ is the conduction of all OS losses.

Under real functioning conditions of the autodyne sensor, the high level of reflected emission is observed on the extremely short distance to the radar object. Under such autodyne operation conditions, it is really acceptable to assume: $\delta(\omega, \tau) = \omega\tau$ [5]. Then, the expression for the phase $\delta(\omega, \tau)$ can be written in the form:

$$\delta(\omega, \tau) = \delta(\chi, \tau_n) = 2\pi(1 + \chi)(N + \tau_n) , \quad (5)$$

where $\tau_n = \omega_0\tau$ is normalized time; $N = \frac{2l}{\lambda}$ is the integer number of half-wavelengths, which falls between a sensor and the radar object.

3 Calculation and analysis of signal characteristics

Main signal autodyne characteristics are functions of relative variations of the amplitude a and the frequency χ of oscillations versus variations of delay time

τ_n of reflected emission [4, 5]. The first function is called the autodyne amplitude characteristic (AAC), while the second function autodyne frequency characteristic (AFC) [6]. For calculation of these characteristics, we rewrite (3) and (4) with account of (5), assuming $\eta = 1$, as follows:

$$a(\tau_n) + \frac{\Gamma\rho}{\alpha} \left(\frac{\gamma B_c(\chi, \tau_n) - B_s(\chi, \tau_n)}{1 - \gamma\rho} + \frac{B_c(\chi, \tau_n)}{\rho} = 0 \right) ; \quad (6)$$

$$\chi(\tau_n) - \Gamma \frac{\gamma B_c(\chi, \tau_n) - B_s(\chi, \tau_n)}{Q_L(1 - \gamma\rho)} = 0 , \quad (7)$$

where

$$B_c(\chi, \tau_n) = \frac{\Gamma - \cos 2\pi(1 + \chi)(N + \tau_n)}{1 + \Gamma^2 + 2\Gamma \cos 2\pi(1 + \chi)(N + \tau_n)} ;$$

$$B_s(\chi, \tau_n) = \frac{\sin 2\pi(1 + \chi)(N + \tau_n)}{1 + \Gamma^2 + 2\Gamma \cos 2\pi(1 + \chi)(N + \tau_n)} ;$$

$\gamma = \frac{\beta}{\alpha}$, $\gamma = \frac{\varepsilon}{Q_L}$ are non-isochrony and non-isodromity coefficients of MO, Q_L is the loaded Q - factor.

The solution of equations (6), (7) we find using mathematical packet MathCAD. For this, at first, we find the solution for autodyne frequency variations χ of the transcendent equation (7) by the secant method or the iteration algorithm realized in the root function. After substitution of obtained values of χ into equation (6), we obtain values of a variable by the same approach.

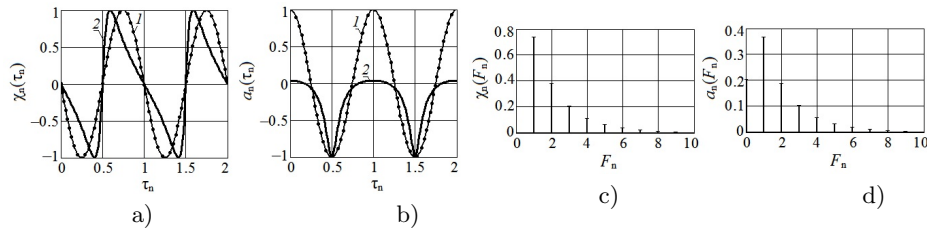


Fig. 2. Plots of AFC $\chi_n(\tau_n)$ (a) and AAC $a_n(\tau_n)$ (b) and their spectra $\chi_n(F_n)$ (c) and $a_n(F_n)$ (d) calculated at $N = 1$; $\gamma = \rho = 0$ and various values of Γ : $\Gamma = 0.01$ (curves 1) and $\Gamma = 0.5$ (curves 2)

Then, performing a search of local extremes in functions $a = a(\tau_n)$ and $\chi = \chi(\tau_n)$ with the help of embedded Maximize (f, x_1, \dots, x_m) function, we obtain maximal values of autodyne variation deviations a_{max} and χ_{max} . After that, we perform normalization of $a = a(\tau_n)$ and $\chi = \chi(\tau_n)$ function with respect to extreme values a_{max} and χ_{max} obtained. At the end, we obtain the required signal characteristics in the normalized form: $a_n = \frac{a(\tau_n)}{a_{max}}$ and $\chi_n = \frac{\chi(\tau_n)}{\chi_{max}}$.

The developed calculation algorithm according to (6) and (7) was verified for obtained results convergence at the small signal, when $\Gamma < 1$, with results of

signal characteristics calculations, which were obtained starting from the small-signal analysis fulfilled in [5, 6].

At first, we perform the analysis for the case of the extremely short distance to the radar object assuming $N = 1$. Then, we reveal the time delay τ influence on features of autodyne response formation assuming $N = 100$. At that, for each case, we introduce variations in inherent MO parameters fulfilling calculations, at first, for isochronous and isodromous case ($\gamma = \rho = 0$), and then for non-isochronous and non-isodromous autodyne MO, when $\gamma \neq 0$ and $\rho \neq 0$.

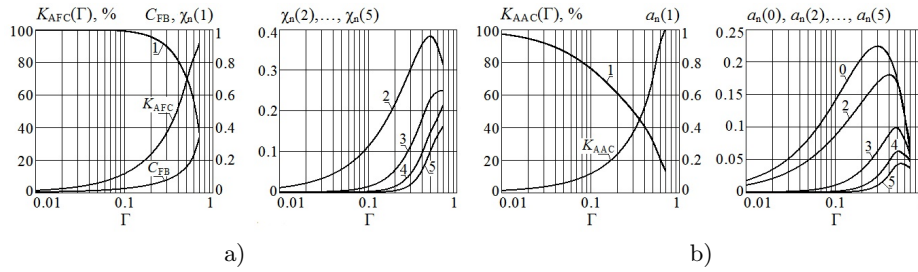


Fig. 3. Plots of coefficients K_{AFC} , K_{AAC} , the FB parameter C_{FB} and the level of spectral components $\chi_n(F_n)$ (a) and $a_n(F_n)$ (b) (*for* $n = 1, 5$) of the autodyne response of the isochronous MO, as well as the average value of $a_n(0)$ versus Γ calculated for $N = 1$; $\gamma = \rho = 0$

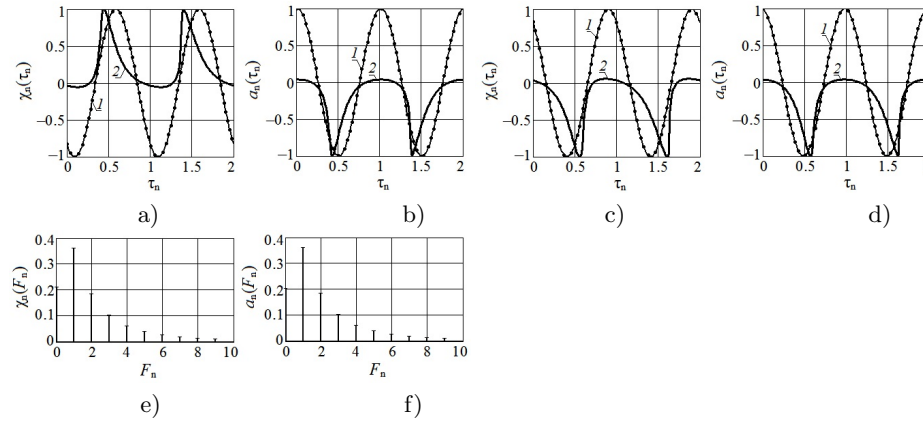


Fig. 4. AFC and AAC (a)(d) and spectra (e), (f) of the autodyne response of non-isochronous and non-isodromous MO calculated at $N = 1$ and various values of Γ : $\Gamma = 0.01$ (curves 1), $\Gamma = 0.5$ (curves 2) and for following parameters: $\gamma = 1.5$; $\rho = 0.1$ (a), (b), (e) and $\gamma = 1.5$; $\rho = 0.1$ (c), (d), (f)

Figures 2 (a), (b) show AFC $\chi_n(\tau_n)$ and AAC $a_n(\tau_n)$ in the form of time-diagrams for the isochronous MO. Plots¹ were calculated at various values of Γ . For strong reflected emission, when $\Gamma = 0.5$, (see curves 2), we perform the expansion of $\chi_n(\tau_n)$ and $a_n(\tau_n)$ into the harmonic Fourier series while Figs. 2 (c), (d) show the corresponding spectra.

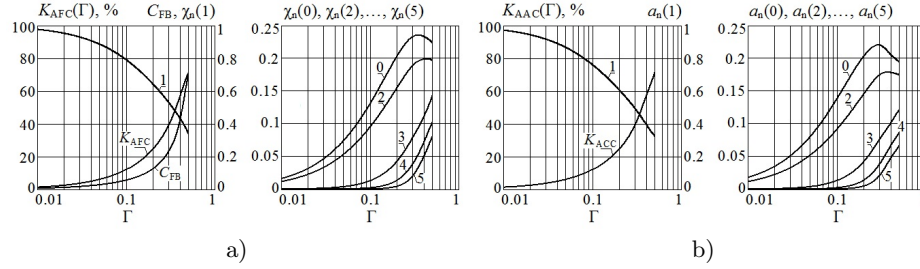


Fig. 5. Plots of coefficients K_{AFC} , K_{ACC} , the FB parameter C_{FB} and the level of spectral components $\chi_n(F_n)$ (a) and $a_n(F_n)$ (b) (*for* $n = 1, 5$) of the autodyne response of the non-isochronous and non-isodromous MO, as well as average values $\chi_n(0)$ and $a_n(0)$ (at $n=0$) versus Γ calculated for $N = 1$; $\gamma = \pm 1.5$; $\rho = \pm 0.1$

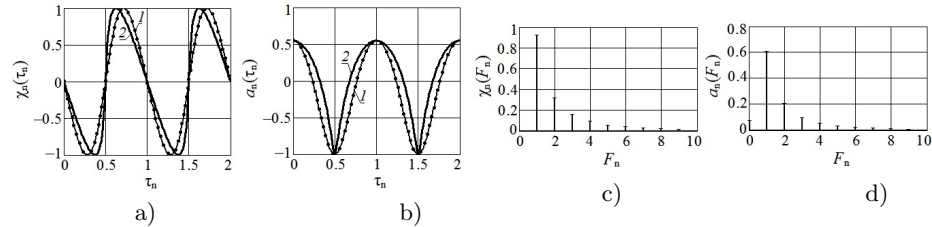


Fig. 6. Plots of AFC (a) and AAC (b) and spectra $\chi_n(F_n)$ (c), $a_n(F_n)$ (d) of the autodyne response of the isochronous MO calculated at $\Gamma = 0.1$; $\gamma = \rho = 0$ and $N : N = 1$ (curves 1) and $N = 100$ (curves 2)

Plots of harmonic coefficients K_{AFC} and K_{ACC} , the level of harmonic components of the autodyne response spectra on the frequency $\chi_n(F_n)$ and of amplitude $a_n(F_n)$ variations, as well as the average value $a_n(0)$ versus the reflection coefficient modulus Γ of the isochronous MO are presented in Figs. 3(a) and (b). Here we show plots of feedback (FB) parameter C_{FB} defining as a product of the delay time of reflected emission by the autodyne frequency deviation [4]. The shape of these plots in Fig. 3 is broken at $\Gamma = 0.7$, for which the instantaneous signal characteristic value jumps begin.

¹ Hereafter, we take the following values: $Q_L = 100$; $\alpha = 0.1$.

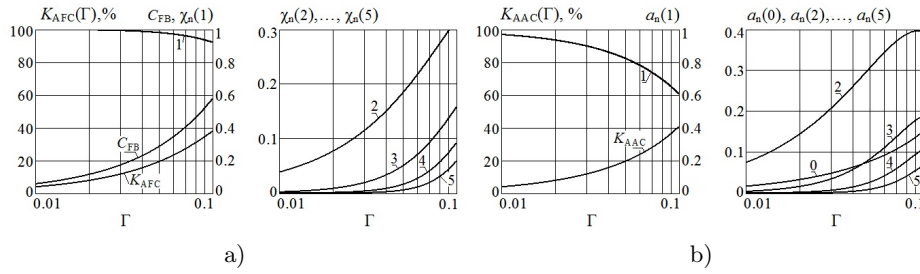


Fig. 7. Plots of coefficients K_{AFC} , K_{ACC} , the FB parameter C_{FB} and the level of spectral components $\chi_n(F_n)$ (a) and amplitudes $a_n(F_n)$ (b) (at $n = 1, \dots, 5$) of spectra and average value (at $n = 0$) of the isochronous MO versus the Γ coefficient calculated for $N = 100$; $\gamma = \rho = 0$

For positive ($\gamma = 1.5$; $\rho = 0.1$) and negative ($\gamma = -1.5$; $\rho = -0.1$) coefficients of non-isochrony and non-isodromity of MO, Figs. 4(a) (d) show AFC $\chi_n(\tau_n)$ and AAC $a_n(\tau_n)$ which are calculated at the previous value of distance ($N = 1$), but at different values of the reflection coefficient Γ : $\Gamma = 0.01$ (curves 1) and $\Gamma = 0.5$ (curves 2).

Spectra $\chi_n(F_n)$ and $a_n(F_n)$ are presented in Figs. 4(e) and (f). Functions $K_{AFC}(\Gamma)$, $K_{ACC}(\Gamma)$ and $C_{FB}(\Gamma)$ are shown in Fig. 5 (a) and (b). Here, we present curves of the harmonic components level $\chi_n(F_n)$, $a_n(F_n)$ (at $n = 1, \dots, 5$) and $\chi_n(0)$, $a_n(0)$ ($n = 0$) versus Γ coefficient. The shape of all these plots, as we see from Fig. 5, are broken at $\Gamma = 0.5$.

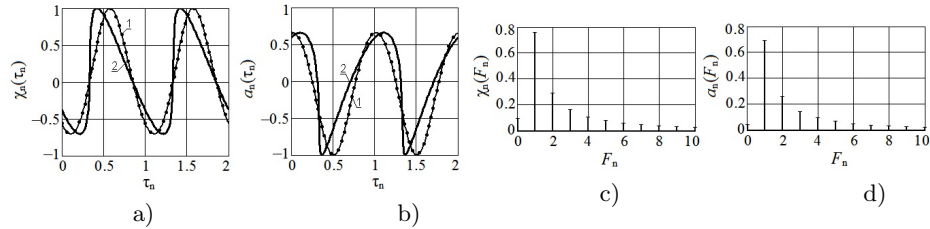


Fig. 8. Plots of AFC (a) and AAC (b) and spectra $\chi_n(F_n)$ (c), $a_n(F_n)$ (d) of the autodyne response of non-isochronous MO calculated at $\Gamma = 0.7$; $\gamma = 1.5$; $\rho = 0.1$ and various N : $N = 1$ (curves 1) and $N = 100$ (curves 2)

The influence of the radar object on the shape and the spectrum of the autodyne signal for the case of isochronous MO is presented on plots in Fig. 6. We observe AFC $\chi_n(\tau_n)$ (a), AAC $a_n(\tau_n)$ (b) and their spectra (c), (d) calculated at $\Gamma = 0.1$ and various values of the half-wavelengths number N from the sensor to the radar object: $N = 1$ (curves 1) and $N = 100$ (curves 2). Figures 7(a) and (b) show the plots of harmonic coefficients K_{AFC} and K_{ACC} , the FB parameter C_{FB} and the level of spectra harmonic components $\chi_n(F_n)$ (a) and $a_n(F_n)$ (b)

(when $n = 1, \dots, 5$), as well as average values of the autodyne response (at $n = 0$) versus of the reflection coefficient modulus Γ .

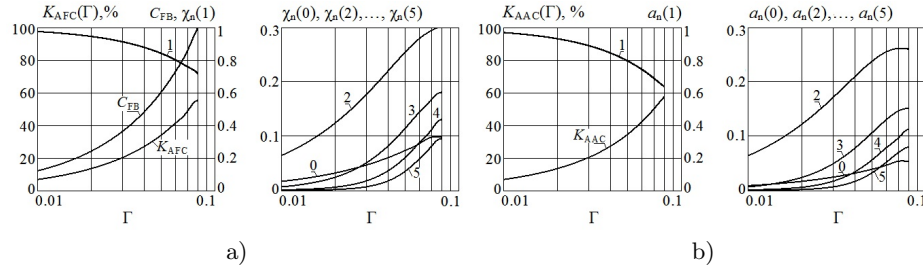


Fig. 9. Plots of coefficients K_{AFC} , K_{AAC} , the FB parameter C_{FB} and the level of spectral components $\chi_n(F_n)$ (a) and amplitudes $a_n(F_n)$ (b) (at $n = 1, \dots, 5$) of spectra and average value (at $n = 0$) of the non-isochronous MO versus the Γ coefficient calculated for $N = 100$; $\gamma = 1.5$; $\rho = 0.1$

For the case of non-isochronous and non-isodronous MO AFC $\chi_n(\tau_n)$, AAC $a_n(\tau_n)$, calculated at various number of half-waves: $N = 1$ (curves 1) and $N = 100$ (curves 2), are presented in plots in Fig. 8 (a) and (b). Spectra calculation results for the case $N = 100$, are presented in Figs. 8(c) and (d). Functions K_{AFC} , K_{AAC} , C_{FB} , as well as levels $\chi_n(F_n)$, $a_n(F_n)$ ($n = 1, \dots, 5$), and $\chi_n(0)$, $a_n(0)$ at ($n = 0$) versus Γ coefficient are presented in Figs. 9(a) and (b). As we see from Fig. 9, in this case plots are broken at $\Gamma=0.08$.

4 Conclusions

The resume of analysis of numerical modeling of the autodyne response formation processes in MO obtained results consist in the following.

Plots of normalized functions of reactive $b_n(\tau_n)$ and resistive $g_n(\tau_n)$ components of the MO load conduction versus the normalized time τ_n are presented in Figs. 2(a) and (b) of the paper [7]. From comparison of these plots with obtained by us curves of AFC $\chi_n(\tau_n)$ and AAC $a_n(\tau_n)$ of the isochronous MO (see Figs. 2(a) and (b)), we see that the last ones practically repeat the former, but with inversion of instantaneous values.

Spectra of reactive $b_n(F_n)$ and active $g_n(F_n)$ load conduction (see Figs. 3(c), (d) of the paper [7]) are similar to the appropriate spectra $\chi_n(F_n)$ and $a_n(F_n)$, which are presented in Figs. 2(c), (d) of the present paper. In addition, as we see from plots comparison in Fig. 4 of the paper [7] and presented by us in Fig. 3, the shape of harmonic coefficients K_b and K_{AFC} , K_g and K_{AAC} practically coincides. At that, the relative values of harmonic levels $b_n(n)$ and $\chi_n(n)$, $g_n(n)$ and $a_n(n)$ and average values $g_n(0)$ and $a_n(0)$ are also in the qualitative agreement.

Characteristic comparison results presented here allow conclusion that autodyne response distortions in the case of strong reflected emission are caused

predominantly by the action of the load nonlinearity rather than the signal restriction by the AE electronic conductance, as was assumed in [1]. We must also note that in the case of isochronous MO, the constant component in $\chi_n(\tau_n)$ autodyne characteristic is absent, as for $b_n(\chi_n)$ component of the load conductance. Signal jumps, as it was mentioned earlier, begin at $\Gamma = 0.7$, at that, the FB parameter $C_{FB} = 0.35$ (see Figs. 3(a), (b)).

MO non-isochrony, as can be seen from comparison of AFC $\chi_n(\tau_n)$ and AAC $a_n(\tau_n)$ in Figs. 2(a), (b) and Figs. 4(a)-(d), causes the phase offset of $\chi_n(\tau_n)$ characteristics by the angle $\theta = \tan^{-1}(\gamma)$, which for chosen parameters ($\gamma = \pm 1.5$) for the positive value of γ , is $\theta \approx 1$, while for the negative values $\theta 1$. MO non-isodromity causes the AAC phase offset by the angle $\psi = \tan^{-1}(\rho)$. Since $Q_{L1} \gg 1$, the angle ψ is comparatively small in value and usually does not exceed ± 0.5 . In here considered case, its value is $\psi \approx 0.1$ at $\rho = 0.1$ (see Fig. 4(b)) and $\psi \approx 0.1$ at $\rho = 0.1$ (see Fig. 4(d)). These phase offsets, as we see from the curves in Figs. 4(a) (d), cause additional clutter of the autodyne response, which are expressed in appearance of characteristic wave tilts to one or another side depending on the ratio of magnitudes and signs of coefficients of non-isochrony γ and non-isodromity ρ of MO.

Besides, MO non-isochrony in the case of strong reflected emission causes on AFC the increase of frequency deviation and appearance of DC component, the sign and magnitude of which depend on the sign and the magnitude of γ coefficient. The first phenomenon leads to increase the autodyne C_{FB} parameter, while the second one lead to the offset of the central frequency of oscillation. Therefore, during increase of the reflection emission level of the isochronous MO, the appearance of signal jumps (see Figs. 5(a), (b)) is observed at lesser reflection coefficient ($\Gamma = 0.5$), than for the isochronous MO ($\Gamma = 0.7$) (see Figs. 3(a), (b)). We should also note that the amplitude spectrum picture for sign change of non-isochrony coefficient γ does not practically change (see Figs. 4(e), (f)). This means that for sign change of γ or movement direction change of the radar object, variations of phase relations occur for harmonic components in the autodyne response spectrum.

From analysis of above cases, it follows that for strong reflected emission, when the reflection coefficient Γ is commensurable with one, jumps in the process of signal formation begin not for $C_{FB} = 1$, as in the case of weak signals [1, 6], but for its lesser values. So, for the case of the isochronous oscillator, jumps begin at $C_{FB} = 0.35$ (see Fig. 3), while for non-isochronous at $C_{FB} = 0.7$ (see Fig. 5).

The increase of radar object distance causes the appropriate growth of the C_{FB} parameter and appearance of signal jumps at lower level of reflected emission. Therefore, at studying of the distance variation influence (the number of half-wavelengths N) on features of the autodyne response formation in the mode of strong reflected emission, the range of analyzed values of the reflection coefficient Γ are proportionally narrowed and passes towards the area of weak signals.

Such a situation found its interpretation in values of Γ chosen for calculations on plots in Figs. 6-9. From these plots, we also see that the presence of the DC component in autodyne frequency variations of the isochronous is absent as in the case of extremely small values of N , whereas for the non-isochronous MO this dependence happens at radar object distance increase. There are no other qualitative differences in features of autodyne signal formation at distance increase.

We should note that obtained results of theoretical studies are well agreed with experimental data published in [1,6]. In addition, they prejudice a correctness of explanation of the autodyne signal distortion reasons, which was suggested in [8-10] without taking into consideration the time delay of reflected emission.

References

1. Votoropin, S. D., Noskov, V. Ya., Smolskiy, S. M.: Modern hybrid-integrated autodyne oscillators of microwave and millimeter ranges and their application. Part 2. Theoretical and experimental investigations (in Russian). *Uspehi sovremennoi radioelektroniki* [Successes of modern electronic engineering], No. 7, 333 (2007)
2. Bogachev, V. M., Lysenko, V. G., Smolskiy, S. M.: Transistor oscillators and autodyne (in Russian). Moskva, Izdat. MEI (1993)
3. Kurokava, K.: Injection Locking of Microwave Solid-State Oscillators. *Proceedings of the IEEE*. Vol. 61, No. 10, 1386-1410 (1973) <https://doi.org/10.1109/PROC.1973.9293>
4. Noskov, V. Ya., Ignatkov, K. A.: Peculiarities of Noise Characteristics of Autodynes under Strong External Feedback. *Russian Physics Journal*. Vol. 56, No. 12, 1445-1460 (2013) <https://doi.org/10.1007/s11182-014-0198-6>
5. Noskov, V. Ya., Ignatkov, K. A.: Dynamic features of autodyne signals. *Russian Physics Journal*. Vol. 56, No. 4, 420-428 (2013) <https://doi.org/10.1007/s11182-013-0051-3>
6. Noskov, V. Ya., Ignatkov, K. A., Smolskiy, S. M.: Autodyne Characteristic Dependence on the UHF Oscillators Inherent Parameters (in Russian). *Radiotecnika*. No. 6, 24-42 (2012)
7. Noskov, V. Ya., Ignatkov, K. A., Smolskiy, S. M.: The role of load variations in the formation of the autodyne response of microwave generators with a strong reflected signal (in Russian). *Radiotekhnicheskie tetradi*, Moscow, MEI-TU, No. 46, 33-36 (2011)
8. Lazarus, M. J., Pantoja, F. R., Somekh, M., Novak, S., Margison, S.: Nw direction-of-motion Doppler detector. *Electronics Letters*. Vol. 16, No. 25, 953-954 (1980) <https://doi.org/10.1049/e1:19800679>
9. Lazarus, M. J., Somekh, M. G., Novak, S., Pantoja, F. R.: Directional Harmonics in Doppler Effect. *Electronics Letters*. Vol. 17, No. 2, 94-96 (1981) <https://doi.org/10.1049/e1:19810068>
10. Lazarus, M. J., Pantoja, F. R., Novak, S., Somekh, M. G.: Sensitivity to Direction of Motion of a Self-Oscillating-Mixer Doppler Radar. *IEE Proc. F: Commun., Radar and Signal Processing*. Vol. 129, No. 4, 233-240 (1982) <https://doi.org/10.1049/ip-f-1:19820035>